Uncertainty-quantifying models for chemical-kinetic rates

By J. Urzay, N. Kseib, P. G. Constantine, D. F. Davidson AND G. Iaccarino

1. Motivation and objectives

In this study, strategies are proposed for modeling the input uncertainties in combustion calculations under chemical-rate uncertainties using as an example hydrogen-oxygen kinetics. For this purpose, this report is divided into the following sections. In Section 2, an assessment is made to ascertain the limitations of state-of-the-art treatments of experimentally-derived chemical-kinetic uncertainties. Based on these limitations, Section 3 proposes a number of modeling strategies and, in particular, an "active-chemical mechanism" concept that is able to treat chemical uncertainties in a general manner and can be used in conjunction with combustion formulations. Finally, conclusions are drawn in Section 4. A follow-up article in this same volume (Urzay *et al.* 2012) provides a turbulent-combustion model that takes the input-uncertainty descriptions proposed in this investigation and uses them in numerical calculations subject to chemical-kinetic uncertainties.

2. Limitations in the use of uncertainty factors for quantifying input uncertainties from chemical-reaction rates

2.1. *State of the art*

Uncertainties in elementary reaction rates of detailed chemical mechanisms have traditionally been reported in terms of temperature-independent and statistically-independent numerical prefactors, which are usually termed "uncertainty factors" or UFs (Baulch *et al.* 2005; Konnov 2008). These uncertainty factors have been used for uncertainty quantification in relatively simple combustion systems and for optimization of chemical mechanisms by assuming that all measurement uncertainties are uncorrelated and temperature-independent, and by lumping all the uncertainties in the exponential prefactors (Reagan *et al.* 2003; Davis *et al.* 2005; Najm *et al.* 2009; Mueller *et al.* 2012). According to classic definitions of UF, the forward rate constant of the reaction step j, $k_{f,j}$ becomes uncertain within the bounds $\ln k_{f,j} \pm \ln \mathrm{UF}_j$. An example of a detailed hydrogen-oxygen chemical mechanism subject to uncertainty factors is shown in Table 1, which will be used in Part II for numerical calculations.

The values of the uncertainty factors are typically reported to account for observed data dispersion in kinetic-isolation measurements, and in particular, for the scatter observed in $\{1/T, \ln k_{f,j}\}$ plots (Baulch *et al.* 2005; Konnov 2008), such as the one depicted in Figure 1(d), which are used conventionally for tabulating rate constants as a function of the temperature T of the tested mixture. Additionally, the probability density function assigned to UF_j is rather arbitrary and very rarely has an experimental justification. As a result of those approaches, an ad-hoc probabilistic description of $\ln k_{f,j}$ is obtained, in which its variability -which is proportional to $\ln \mathrm{UF}_j$- neither depends on temperature

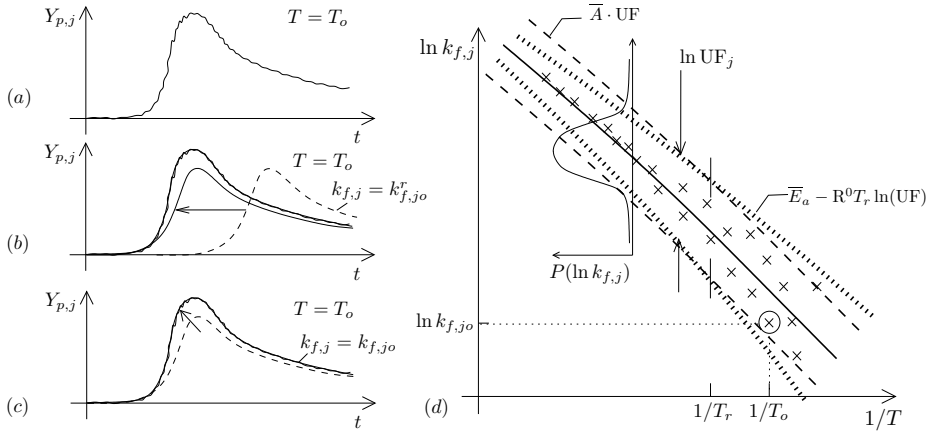

FIGURE 1. Sketch of a typical sequence followed to derive a rate constant k_f of an elementary step from shock-tube kinetic-isolation experiments. Details of each stage are given in the main text.

in a physically meaningful manner nor is correlated with any other reaction steps in the chemical mechanism.

The objective of the remainder of this document is to identify the main conceptual flaws of these approaches and to propose more accurate methodologies for quantifying uncertainties in chemical reaction rates.

2.2. *The Arrhenius approximation and uncertainties in chemical mechanisms*

Consider a chemical mechanism given by the set of $j = 1, 2...M$ elementary steps $\sum_{i=1}^{N} \nu'_{ij} \mathcal{R}_i \rightleftharpoons \sum_{i=1}^{N} \nu''_{ij} \mathcal{R}_i$, with $\mathcal{R}$ the chemical symbol of species i, N the number of species, ν'_{ij} the stoichiometric coefficient of the reactant i in the step j on the reactants side, and ν''_{ij} the stoichiometric coefficient of the reactant i in the step j on the products side. The net rate of mass production of species i and the rate of thermal power released by chemical reactions are given by

$$\dot{w}_i = W_i \sum_{j=1}^{M} (\nu''_{ij} - \nu'_i) \left[k_{f,j} \prod_{i=1}^{N} \left(\frac{\rho Y_i}{W_i} \right)^{\nu'_{ij}} - k_{b,j} \prod_{i=1}^{N} \left(\frac{\rho Y_i}{W_i} \right)^{\nu''_{ij}} \right], \tag{2.1}$$

and

$$\dot{w}_T = - \sum_{i=1}^{N} h_i^0 \dot{w}_i, \tag{2.2}$$

respectively, where ρ is the gas density. In this formulation, Y_i, W_i and h_i^0 are, respectively, the mass fraction, molecular weight and enthalpy of formation of species i. Additionally, the constants $k_{f,j}$ and $k_{b,j}$ are, respectively, the forward and backwards specific reaction-rate constants of the reaction j, which are related by the equilibrium constant K_j as $\mathrm{K}_j = k_{f,j}/k_{b,j}$. In the Arrhenius approximation, the reaction-rate constants follow the expression

$$k_{f,j} = A_j T^{n_j} \mathrm{e}^{-E_{a,j}/\mathrm{R}^0 T}, \tag{2.3}$$

where A_j is the exponential prefactor, n_j is the temperature exponent, T is the temperature, R^0 is the universal gas constant, and $E_{a,j}$ is the activation energy. In this

Reaction	UF	Reference
Hydrogen-oxygen chain		
1. $H + O_2 \rightleftharpoons OH + O$	1.1	Hong *et al.* (2011)
8. $H_2O + O \rightleftharpoons OH + OH$	1.5	Konnov (2008)
9. $H_2 + O \rightleftharpoons H + OH$	1.3	Konnov (2008)
10. $H_2 + OH \rightleftharpoons H_2O + H$	2.0	Konnov (2008)
Direct recombination		
2. $H + O_2 + M \rightleftharpoons HO_2 + M$	1.3	Konnov (2008)
7. $H + OH + M \rightleftharpoons H_2O + M$	2.0	Konnov (2008)
18. $H + H + M \rightleftharpoons H_2 + M$	2.0	Konnov (2008)
19. $O + O + M \rightleftharpoons O_2 + M$	2.0	Konnov (2008)
20. $H + O + M \rightleftharpoons OH + M$	3.0	Konnov (2008)
Hydroperoxyl reactions		
5. $HO_2 + OH \rightleftharpoons H_2O + O_2$	1.3	Hong *et al.* (2011)
11. $HO_2 + H \rightleftharpoons OH + OH$	2.0	Konnov (2008)
12. $HO_2 + H \rightleftharpoons H_2O + O$	3.0	Konnov (2008)
13. $HO_2 + H \rightleftharpoons H_2 + O_2$	2.0	Konnov (2008)
14. $HO_2 + O \rightleftharpoons OH + O_2$	1.2	Konnov (2008)
Hydrogen-peroxide reactions		
3. $H_2O_2 + M \rightleftharpoons OH + OH + M$	1.2	Hong *et al.* (2011)
4. $H_2O_2 + OH \rightleftharpoons H_2O + HO_2$	1.3	Hong *et al.* (2011)
6. $HO_2 + HO_2 \rightleftharpoons H_2O_2 + O_2$	2.5	Konnov (2008)
15. $H_2O_2 + H \rightleftharpoons HO_2 + H_2$	3.0	Konnov (2008)
16. $H_2O_2 + H \rightleftharpoons H_2O + OH$	2.0	Konnov (2008)
17. $H_2O_2 + O \rightleftharpoons HO_2 + OH$	3.0	Konnov (2008)

TABLE 1. Reactions and uncertainty factors in measured reaction constants for the reference mechanism (Hong *et al.* 2011). Note that the uncertainty factor UF_j of a rate constant $\overline{k}_{f,j}$ is such that $\overline{k}_{f,j}\mathrm{UF}_j$ and $\overline{k}_{f,j}/\mathrm{UF}_j$ are upper and lower bounds of $k_{f,j}$. This mechanism has 3 parameters $\times$11 Arrhenius steps + 12 parameters $\times$6 recombination non-Arrhenius steps + 6 parameters $\times$3 non-Arrhenius steps = 123 kinetic parameters.

model, $A_j T^{n_j}$ is proportional to a collision frequency that depends on the effective collision cross-section, and $\exp(-E_{a,j}/\mathrm{R}^0 T)$ is proportional to the fraction of gas molecules moving with a kinetic energy larger than the Arrhenius activation energy.

In most instances, the parameters A_j, n_j and $E_{a,j}$ are subject to uncertainties. In theoretical calculations, there are uncertainties in parameters for collision-integral calculations. In experiments, uncertainties are induced by the transience and complexity of the systems, which often prevent isolation of individual rate parameters. Nonetheless, the accuracy of rate measurements has increased to a level in which uncertainties can be lowered to 10% in important elementary reactions (Hong 2010). The uncertainties in the Arrhenius parameters render the chemical source terms (2.1) and (2.2) uncertain, the treatment of which is deferred to Part II.

In order to ascertain the effects of the uncertainties of the kinetic parameters on the rate constant, consider a dimensionless version of (2.3) given by $\hat{k}_f = \hat{A}^\star \theta^{\hat{n}} \mathrm{e}^{-\hat{\beta}/\theta}$, where $\theta = T/T_{fl}$ is a dimensionless temperature normalized with the flame temperature T_{fl} (which needs not to be specified at this point), $\hat{\beta} = \beta - \overline{\beta}$ is the nondimensional variation of the activation energy with respect to its mean value $\overline{\beta} = \overline{E}_a/\mathrm{R}^0 T_{fl}$, $\hat{n} = n - \overline{n}$ is the variation of temperature exponent referred to the mean value $\overline{n}$, $\hat{A}^\star = A^\star/\overline{A}^\star$ is the uncertain

collision frequency normalized with its mean value $\overline{A}^\star$, with $A^\star = AT_{fl}^{\hat{n}}$, and $\hat{k}_f$ is the uncertain reaction rate normalized with the reference reaction rate $\overline{k}_f = \overline{A}^\star \theta^{\overline{n}} \exp(-\overline{\beta}/\theta)$ based on the mean parameters and on the reference-temperature. In this way, $\hat{k}_f = 1$ in nominal conditions, which correspond to $\hat{\beta} = \hat{n} = 0$ and $\hat{A}^\star = 1$. The parameter β is typically referred to as the Zel'dovich number in combustion literature. Because of the large value of the overall β in combustion systems, small variations in temperature above or below a critical crossover temperature can cause order-unity variations in the reaction rates, which tend to be sufficient for extinguishing or igniting flames. Here the effect of temperature is set aside. Instead, attention is paid to uncertainties in kinetic parameters that produce uncertainties of order unity in the rate constant, $\hat{k}_{f,j} - 1 = O(1)$, thereby potentially making the combustion system uncertainly close to critical points.

Based on this formulation, uncertainties of $O(\mathrm{UF})$ in the dimensionless pre-exponential factor $\hat{A}^\star$ produce uncertainties of the same order of magnitude in the dimensionless rate constant, $\hat{k}_f = 1 + O(\mathrm{UF})$. For inducing uncertainties of $O(\mathrm{UF})$ in $\hat{k}_f$, the uncertainties in the activation energy need to be such that $\hat{\beta}/\theta = O(\ln \mathrm{UF})$, or equivalently, the variations in the Zel'dovich number β caused by activation-energy uncertainties need to be $\beta - \overline{\beta} \sim (T/T_{fl}) \ln \mathrm{UF}$. In dimensional notation, standard deviations σ_{E_a} of order $\mathrm{R}^0 T \ln \mathrm{UF}$ in the activation energy produce the same overall uncertainty in the rate constant k_f that would be obtained by varying the pre-exponential factor A in amounts of $O(A \cdot \mathrm{UF})$. A characteristic temperature $T_r = \sigma_{E_a}/\mathrm{R}^0 \ln \mathrm{UF}$ can be defined such that, for $T < T_r$, the effect of the activation-energy uncertainty in $k_{f,j}$ overwhelms the effect of the uncertainty of $O(A \cdot \mathrm{UF})$ in the pre-exponential factor, as depicted in Figure 1(d). Additionally, since the chemical time becomes longer and more sensitive to E_a for decreasingly small temperatures, the effects of the activation-energy uncertainty in $k_{f,j}$ are larger at low temperatures.

In addition to parametric uncertainties, there exist epistemic uncertainties associated with the Arrhenius formula (2.3). Even though (2.3) can be derived from first principles of statistical mechanics for $n = 1/2$ and for collision processes that actually occur at the molecular scale, the rates of many elementary steps do not follow the Arrhenius formula (2.3), as for instance the rates of the steps 2-4, 6, 7, 9, and 18-20 in Table 1. Additionally, an underlying hypothesis of the Arrhenius approximation (2.3) is that local thermodynamic equilibrium occurs, in that it is assumed that a unique local temperature can be defined; the accuracy of this assumption is degraded in high-speed, very hot reacting systems such as strong detonations or atmospheric-reentry flows.

Chemical-kinetic mechanisms are also subject to structural uncertainties. In well-researched mechanisms, such as the hydrogen-oxygen mechanism shown in Table 1, this degree of epistemic uncertainty is relatively small, in that the overall structure of the kinetics has been successfuly tested in many studies (Konnov 2008). However, the use of reduced hydrogen-oxygen combustion kinetics - of interest for saving computational cost in direct numerical simulations - can introduce a large degree of structural uncertainties if, for instance, the reduced description does not account for high-pressure dissociation effects that in particular scenarios may be important for reignition. In fact, the effects of epistemic uncertainties may as well overwhelm any influences of aleatory uncertainties in the mechanism; for many heavy hydrocarbons such as JP-7, whose surrogate has approximately 111 species and 784 steps, the chemical mechanisms are still under structural development and much research on them remains to be done.

2.3. *Chemical-kinetic measurement uncertainties in shock tubes*

As noted above, the uncertainty factors UF_j are introduced to represent the data scatter in experimental results (Baulch *et al.* 2005; Konnov 2008). A typical instrument used for determining reaction rates is the shock tube (Davidson & Hanson 2004). In shock tubes, a driver section is filled with an inert high-pressure gas separated by a diaphragm from the driven test mixture. When the diaphragm is relieved, a shock wave propagates into the driven mixture. The incident or reflected passage of the shock wave leaves the mixture at the test pressure and temperature, which eventually leads to autoignition in a mostly transport-less environment. That the experiments should preferably be free of advection and diffusion transport (which is present in flames) is motivated by the fact that uncertainties in mixing and fluid mechanics would add more complexity in the uncertainty-propagation dynamics. The hypothesis that transport phenomena in shock tubes are negligible during the short test times ($\lesssim$1-3 ms) has generally be found to be valid, though turbulence and boundary-layer effects can become significant in some cases at longer test times (Davidson & Hanson 2004).

Kinetic rates can be determined in shock tubes by measuring concentration time-histories through laser-absorption spectroscopy techniques (Hong 2010). Figure 1(a) shows a sketch of a typical concentration time-history of the monitored species $Y_{p,j}$ during an kinetic-isolation experiment at temperature T_o. Note that the choice of the monitored species $Y_{p,j}$ depends on the step j which rate is to be measured. After the measurements $\{t, Y_{p,j}\}_{T=T_o}$ have been collected, numerical calculations of an isochoric accumulation-reaction problem of the type

$$\mathcal{D}_s Y_i = \dot{w}_i \quad \text{and} \quad \mathcal{D}_e T = \dot{w}_T \tag{2.4}$$

are performed, with $i = 1, \ldots N$, and where $\dot{w}_i$ and $\dot{w}_T$ are given by (2.1) and (2.2). Equations (2.4) are subject to $Y_i = Y_{i,o}$ and $T = T_o$ at $t = 0$. In this formulation, Y_i is the mass fraction, T is the temperature, $\mathcal{D}_s = \rho d/dt$, $\mathcal{D}_e = \rho c_p d/dt$, and ρ is the mixture density. Similarly, $c_p = \sum_{i=1}^{N} \int_{T_{ref}}^{T} Y_i c_{pi}(T) dT$ is the constant-presure specific heat of the mixture. This formulation describes a homogeneous explosive mixture at rest, which is, to some extent, representative of the region downstream from the shock wave in a reference frame moving with the velocity of the gas behind the shock wave.

To obtain a value of the measured rate constant $k_{f,j}$, in a first step equations (2.4) can be integrated with a reference mechanism to ascertain the level of impurities in the shock tube, in such a way that the initial conditions for the radical pool are varied to achieve matching between the numerical curve and the experimental profile of the monitored species at the rising point, as depicted in Figure 1(b). The second step involves performing numerical calculations of the same problem (2.4) with the reference mechanism and the initial concentration of impurities calculated in the previous step, by varying the target rate constant $k_{f,j}$ to fully match the experimental profile. It should be emphasized that this procedure requires that i) a reference rate constant $k^r_{f,j}$ is known and can be used initially in the steps depicted in Figure 1(b,c), and ii) the time evolution of the monitored species $Y_{p,j}$ is most sensitive to the target rate constant $k_{f,j}$. See, for instance, Davidson *et al.* (1996) and Hong (2010) for practical implementations of this sequence.

A usual method for retrieving uncertainties from shock-tube measurements of rate constants consists of identifying the experimental variable which the target result is most sensitive to, and then calculating the solution to the problem (2.4) with a reference mechanism, in which the experimental variable is perturbed by the maximum uncertainty of the corresponding instrument that measures it. For a characteristic temperature, the

perturbation in the resulting value of the modified reaction rate is typically listed as the uncertainty factor UF_j of that reaction (Hong 2010).

2.4. *Limitations of uncertainty factors*

In summary, the following limitations $\mathcal{L}_1 - \mathcal{L}_4$ should be kept in mind when using tabulated uncertainty factors:

Limitation $\boldsymbol{\mathcal{L}_1}$) The uncertainties in the Arrhenius activation energies and temperature exponents are typically ignored in the reference literature. In particular, the importance of uncertainties in the Arrhenius activation energies of rate-determining steps may be of some relevance near critical phenomena in combustion, in which small variations of temperature can lead to extinction or ignition events because of the strong exponential non-linearity of the chemical rate.

Limitation $\boldsymbol{\mathcal{L}_2}$) The techniques used for rate measurements, which usually rely on the detection of radical traces by using laser absorption spectroscopy (Davidson *et al.* 1996), are applicable only in a limited range of temperatures, in that the population of radicals becomes increasingly small for decreasing temperatures. Additionally, for measurements performed near crossover temperatures, the residence time of the shocked mixture in the shock tube becomes increasingly large, which results in the measurements being influenced by non-ideal pressure-rise effects (Hong 2010), thereby adding more uncertainty in the low-temperature data.

Limitation $\boldsymbol{\mathcal{L}_3}$) Residual impurities, which may inadvertently remain from previous experiments in the shock tube, can degrade the accuracy of rate measurements based on radical-absorption diagnostics (Davidson & Hanson 2004). Kinetic-isolation experiments are typically performed in dilute conditions. As a result, the presence of small amounts of impurities in the shock tube can interfere with the chemical kinetics of the main reactants.

Limitation $\boldsymbol{\mathcal{L}_4}$) Experiments for isolating the kinetics of specific steps can be designed to give accurate rates under negligible influences of the remaining steps. Despite the existence of these observation windows, cross-correlations among the errors in the measurements of elementary rates become important when the timescale of the target step becomes of the same order as the time scales of the competing steps, in which case the measurement of the target rate necessitates of an accurate measurement of the competing rates. In hydrogen combustion, this interference becomes evident at near-crossover temperatures at which the branching kinetics are as slow as the recombination of radicals (Hong 2010). The mathematical definition of the cross-correlations among uncertainties in reaction rates is given in the following section. The extent to which these cross-correlations have an impact in overall combustion calculations under chemical uncertainties is still under discussion (Sheen & Wang 2011).

With all these limitations in mind, a general framework for inferring uncertainties in reaction rates is proposed in what follows.

3. Methods for quantifying uncertainties in chemical rates

Consider, without any loss of generality, a chemical mechanism in which the kinetic parameters are given by the general expression

$$\boldsymbol{\mathcal{S}} = \boldsymbol{\mathcal{F}}(\boldsymbol{\xi}), \tag{3.1}$$

where $\boldsymbol{\mathcal{S}} = [\boldsymbol{\mathcal{S}_1}, \boldsymbol{\mathcal{S}_2}, \dots, \boldsymbol{\mathcal{S}_M}]$ is a vector that concatenates all the individual vectors $\boldsymbol{\mathcal{S}_j} = [\ln B_j, n_j, E_{a,j}, \dots]$, which contain all kinetic parameters of each elementary step.

Here $B_j = A_j T_c^{n_j}$, with T_c an arbitrary characteristic temperature used for reducing A_j to avoid physical inconsistencies in (2.3) when A_j and n_j are random (i.e. A_j changes physical units as n_j varies). In general, the covariance matrix of $\boldsymbol{\mathcal{S}}$ is full, with the off-diagonal terms indicating cross-correlations among kinetic parameters. Similarly, $\boldsymbol{\xi}$ is a vector of independent random variables -which need not be specified in this general formulation-, and $\boldsymbol{\mathcal{F}}$ is an operator which is nonlinear in the most general setting. The vector of rate constants $\boldsymbol{\mathcal{K}} = [k_{f,1}, \dots k_{f,M}]$ is obtained by using the transformation

$$\ln \boldsymbol{\mathcal{K}} = \boldsymbol{\mathcal{G}}[\boldsymbol{\mathcal{S}}(\boldsymbol{\xi}), p, T], \tag{3.2}$$

where p is the pressure and $\ln \boldsymbol{\mathcal{K}}$ indicates the logarithm of the components of $\boldsymbol{\mathcal{K}}$. Similarly, $\boldsymbol{\mathcal{G}}$ is generally a non-linear operator.

For steps that follow the Arrhenius law (2.3), the operator $\boldsymbol{\mathcal{G}}$ becomes linear and pressure-independent,

$$\ln k_{f,j} = \mathcal{G}_j[\boldsymbol{\mathcal{S}_j}(\boldsymbol{\xi}), T] = \ln B_j(\boldsymbol{\xi}) + n_j(\boldsymbol{\xi}) \ln(T/T_c) - E_{a,j}(\boldsymbol{\xi})/\mathrm{R}^0 T. \tag{3.3}$$

For steps that do not follow the Arrhenius law (2.3), the operator $\boldsymbol{\mathcal{G}}$ is non-linear and can become as complicated as

$$\ln k_{f,j} = \mathcal{G}_j[\boldsymbol{\mathcal{S}_j}(\boldsymbol{\xi}), T] = \ln \left[A_{j,1}(\boldsymbol{\xi}) \mathrm{e}^{-\frac{E_{a,j,1}(\boldsymbol{\xi})}{\mathrm{R}^0 T}} + A_{j,2}(\boldsymbol{\xi}) \mathrm{e}^{-\frac{E_{a,j,2}(\boldsymbol{\xi})}{\mathrm{R}^0 T}} \right], \tag{3.4}$$

for steps 4, 6 and 9 in Table 1, and

$$\ln k_{f,j} = \mathcal{G}_j[\boldsymbol{\mathcal{S}_j}(\boldsymbol{\xi}), p, T] = \ln \left(\frac{\eta_{\mathrm{M}} k_{f,j,0} F_c^{\{1+[(0.75-1.27 \ln F_c)^{-1} \ln(k_{f,j,0}[\mathrm{M}]/k_{j,\infty})]^2\}^{-1}}}{1 + [\mathrm{M}] k_{f,j,0}/k_{j,\infty}} \right) \tag{3.5}$$

for the direct-recombination reactions in Table 1, where $\eta_{\mathrm{M}}(\boldsymbol{\xi})$ and $[M] = p/\mathrm{R}^0 T$ are, respectively, the collision efficiency and concentration of the background collider, $k_{f,j,0} = B_{j,0}(\boldsymbol{\xi})(T/T_c)^{n_{j,0}(\boldsymbol{\xi})} \exp[-E_{a,j,0}(\boldsymbol{\xi})/\mathrm{R}^0 T]$ is the rate constant at low pressure, $k_{f,j,\infty} = B_{j,\infty}(\boldsymbol{\xi})(T/T_c)^{n_{j,\infty}(\boldsymbol{\xi})} \exp[-E_{a,j,\infty}(\boldsymbol{\xi})/\mathrm{R}^0 T]$ is the rate constant at high pressure, and F_c is a Troe fall-off factor that helps matching the high and low pressure rates and is normally given by $F_c = a(\boldsymbol{\xi}) \exp[-T/T_1(\boldsymbol{\xi})] + [1 - a(\boldsymbol{\xi})] \exp[-T/T_2(\boldsymbol{\xi})] + b(\boldsymbol{\xi}) \exp[-T/T_3(\boldsymbol{\xi})]$. Note that expression (3.5) contains 12 potentially aleatory parameters.

The obtention of the operator $\boldsymbol{\mathcal{F}}$ in (3.1) is central to uncertainty quantification in chemical rates. In some cases, an expression of $\boldsymbol{\mathcal{F}}$ can be obtained in closed form, but in general $\boldsymbol{\mathcal{F}}$ needs to be evaluated numerically. For instance, $\boldsymbol{\mathcal{F}}$ could be given by a polynomial-chaos expansion for each component of the random vectors $\boldsymbol{\mathcal{S}_j}$ in terms of $\boldsymbol{\xi}$, or by using a Cholesky decomposition of the covariance matrix. Alternatively, the expression (3.1) can be evaluated numerically by using a Markov-Chain Monte Carlo (MCMC) method to construct a posterior distribution, as described below. In order to overcome the limitations $\mathcal{L}_1 - \mathcal{L}_4$ outlined above, four different methods $\mathcal{M}_1 - \mathcal{M}_4$ for obtaining $\boldsymbol{\mathcal{F}}$ and inferring uncertainties in reaction rates are proposed in what follows. It is shown below that the first three approaches $\mathcal{M}_1 - \mathcal{M}_3$ are particular cases of a more general framework $\mathcal{M}_4$, which is herein referred to as the *active chemical mechanism*.

Method $\boldsymbol{\mathcal{M}_1}$) The simplest approach consists of collecting uncertainty factors from existing literature (Baulch *et al.* 2005) for each rate constant $k_{f,j}$ and assuming a temperature-independent, uncorrelated noise ϵ_j, whose standard deviation is proportional to UF_j, and which spans along the $\ln k_{f,j}$ axis in the $\{1/T, \ln k_{f,j}\}$ plane, as depicted in Figure 1(d). By doing this, the operator $\boldsymbol{\mathcal{F}}$ in (3.1) becomes linear and the

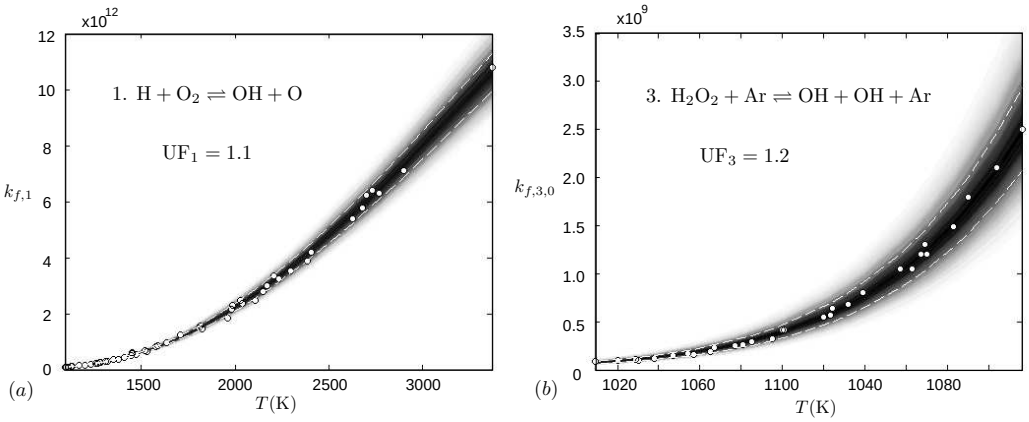

FIGURE 2. Conditional probability density function (PDF) $P(k_{f,j}|T)$ of the forward rate constants $k_{f,1}$ and $k_{f,3,0}$ (in $\mathrm{cm}^3/\mathrm{s}{\cdot}\mathrm{mol}$) of steps 1 and 3 in Table 1. The PDFs were obtained by using method $\mathcal{M}_2$ to infer the statistical distributions of A_1, $E_{a,1}$, $A_{3,0}$ and $E_{a,3,0}$. The dark regions indicate high probability. The white dashed lines indicate one standard deviation with respect to the mean. The white dots correspond to shock-tube measurements taken from Hong (2010).

covariance matrix of $\boldsymbol{\mathcal{S}}$ becomes diagonal, where its only non-zero terms are of the form $(1/4)\ln^2 \mathrm{UF}_j$. If ϵ_j is taken to be Gaussian, then $k_{f,j}$ has a lognormal probability density function with mean $\overline{k}_{f,j}$ and variance $\sigma^2_{\epsilon_j} = (1/4)\ln^2 \mathrm{UF}_j$, which gives

$$k_{f,j} = \xi_j \overline{k}_{f,j}, \quad \text{with} \quad \ln \xi_j \sim \mathcal{N}\left(0, \frac{\ln^2 \mathrm{UF}_j}{4}\right), \quad j = 1, \ldots M. \tag{3.6}$$

In this formulation, ξ_j is a lognormal random variable and $\mathcal{N}$ indicates a normal probability distribution. The symbol $\overline{k}_{f,j}$ denotes the nominal rate constants in Table 1, but it is also the conditional median of the distribution of rate constants (not to be confused with the mean). The random variables ξ_j, $j = 1, ...M$, are taken here to be statistically independent. This model is intended to represent uncertainties for isolated reactions in which the data scatter is mostly temperature-independent in the $\{1/T, \ln k_{f,j}\}$ plane, in such a way that the deviations with respect to the nominal values become multiplicative in the $\{T, k_{f,j}\}$ plane; this is clearly not always the case (Davidson *et al.* 1996). Note that, depending on the analyzed data set, the unbiased variance estimator of the data may not be equal to the variance given by the uncertainty factor, since the former only accounts for data scatter and the latter is expected to account for all experimental uncertainties. If the unbiased variance estimator is much larger than the variance given by the uncertainty factor, then the former should be used as a variance in (3.6).

Method $\mathcal{M}_1$ provides the probability density function of the rate constant $P(k_{f,j})$, with each realization of $k_{f,j}$ being a temperature-uniform multiplicative factor of the previous ones. This method is limited by $\mathcal{L}_1 - \mathcal{L}_4$ listed above, in that it does not take into account measurement-uncertainty variations with temperature, it does not account for cross-correlation among measurement errors of different elementary rates, it assumes as certain the values of the activation energy and temperature exponent for every step, and it does not model the effects of residual impurities in the rate measurements. Additionally, in this model the uncertainty of $k_{f,j}$ is biased towards values of the rate constant larger than the nominal value $\overline{k}_{f,j}$ because of the normality of the noise. This model has been

widely used to generate input chemical uncertainties in earlier works on combustion calculations (Reagan *et al.* 2003; Mueller *et al.* 2012).

Method $\mathcal{M}_2$) This second method builds on $\mathcal{M}_1$ by assuming that the three Arrhenius parameters A_j, n_j and $E_{a,j}$ in (2.2) become uncertain. In this way, the rate constant is given by

$$k_{f,j} = B_j(\boldsymbol{\xi_j})(T/T_c)^{n_j(\boldsymbol{\xi_j})}\mathrm{e}^{-E_{a,j}(\boldsymbol{\xi_j})/\mathrm{R}^0 T}, \quad j = 1, \dots M. \tag{3.7}$$

where $\boldsymbol{\xi_j} = [\xi_{j,1}, \xi_{j,2}, \xi_{j,3}]^{\mathrm{T}}$ is a vector of random variables. Equation (3.7) implies that the operator $\mathcal{G}_j$ defined in (3.2) is linear in the kinetic parameters, and additionally, that $\ln B_j = \ln A_j T_c^{n_j}$, n_j, $E_{a,j}$ and $\boldsymbol{\xi_j}$ have Gaussian probability density functions if the noise ϵ_j along the $\ln k_{f,j}$ axis in the $\{1/T, \ln k_{f,j}\}$ plane is Gaussian. Under these assumptions, the operator $\boldsymbol{\mathcal{F}}$ in (3.1) is linear and the covariance of the vector of kinetic parameters $\boldsymbol{\mathcal{S}}$ becomes block diagonal, with the zeros indicating the absence of cross correlations among kinetic parameters of different steps. In particular, since (3.7) becomes linear after a logarithmic transformation, the vector of kinetic parameters $\boldsymbol{\mathcal{S}_j}$ can be expanded as $\boldsymbol{\mathcal{S}_j} = \overline{\boldsymbol{\mathcal{S}}}_{\boldsymbol{j}} + \boldsymbol{\alpha}_j \boldsymbol{\xi_j}$, where $\overline{\boldsymbol{\mathcal{S}}}_{\boldsymbol{j}} = (\boldsymbol{\mathcal{G}_j}^{\mathrm{T}} \boldsymbol{\mathcal{G}_j})^{-1} \boldsymbol{\mathcal{G}_j}^{\mathrm{T}} \boldsymbol{X_j}$ is the least-squares estimator, and $\boldsymbol{\alpha_j}$ is an upper-triangular matrix that results from the Cholesky decomposition of the covariance matrix $\mathrm{cov}(\boldsymbol{\mathcal{S}_j}) = \sigma^2_{\epsilon_j} (\boldsymbol{\mathcal{G}_j}^{\mathrm{T}} \boldsymbol{\mathcal{G}_j})^{-1}$, namely, $\mathrm{cov}(\boldsymbol{\mathcal{S}_j}) = \boldsymbol{\alpha_j} \boldsymbol{\alpha_j}^{\mathrm{T}}$. In this formulation, $\boldsymbol{\mathcal{G}_j}$ is a $\mathbb{R}^{K \times 3}$ coefficient matrix which rows are given by (3.3) evaluated at the test temperatures, and $\boldsymbol{X_j} = [\ln k_{f,j,1}(T_1), \dots \ln k_{f,j,K}(T_K)]^{\mathrm{T}}$ is a vector composed of the K measured data points. Note however that, since the noise has been modeled to have a constant variance, this linear regression model provides a reaction-rate variance $\mathrm{var}[\ln k_{f,j}]$ which depends on temperature. The kinetic parameters in Figure 2(a,b) were obtained using this method.

The operator $\boldsymbol{\mathcal{G}}$ is non-linear for the recombination steps and for the steps 4, 6 and 9 in Table 1, so that the individual Arrhenius parameters are not necessarily Gaussian-distributed and the strategy outlined above is not applicable. Similarly, the operator $\boldsymbol{\mathcal{F}}$ in (3.1) is non-linear for these steps, and more general techniques are required to obtain the statistical description of the kinetic parameters. For this purpose, the Bayesian method can be employed to infer the probabilistic distributions of the kinetic parameters as follows. The objective of the Bayesian method is to find the input-parameter vector $\boldsymbol{\mathcal{S}_j}$ that brings the model into agreement with the measurements up to the imposed noise ϵ_j. In mathematical terms, this can be expressed as $\mathcal{G}_j(\boldsymbol{\mathcal{S}_j}) = \boldsymbol{X_j} + \epsilon_j$, thereby implying that $\mathcal{G}_j(\boldsymbol{\mathcal{S}_j}) - \boldsymbol{X_j}$ has the same distribution as the noise ϵ_j, in accord with Figure 1(d).

The inference of the input parameters can be performed by using Bayes' rule,

$$P(\boldsymbol{\mathcal{S}_j}|\boldsymbol{X_j}) = cP(\boldsymbol{X_j}|\boldsymbol{\mathcal{S}_j})P(\boldsymbol{\mathcal{S}_j}). \tag{3.8}$$

In this formulation, $P(\boldsymbol{\mathcal{S}_j}|\boldsymbol{X_j})$ is the posterior density, or equivalently, the occurrence probability of the parameter-vector $\boldsymbol{\mathcal{S}_j}$ conditioned on the data set $\boldsymbol{X_j}$. Similarly, the symbol $P(\boldsymbol{X_j}|\boldsymbol{\mathcal{S}_j})$ denotes the likelihood function, or equivalently, the occurrence probability of the measurements $\boldsymbol{X_j}$ conditioned on the input-parameter vector $\boldsymbol{\mathcal{S}_j}$. Additionally, $P(\boldsymbol{\mathcal{S}_j})$ is the prior or occurrence probability of $\boldsymbol{\mathcal{S}_j}$, which can be assumed to be given by a uniform density in the input-parameter space. Finally, c is a normalizing constant that ensures that the product of the likelihood and the prior is a probability density function. Since both $P(\boldsymbol{\mathcal{S}_j})$ and c are constants over the parameter space, we can rewrite Bayes' rule as $P(\boldsymbol{\mathcal{S}_j}|\boldsymbol{X_j}) \propto P(\boldsymbol{X_j}|\boldsymbol{\mathcal{S}_j})$, where $P(\boldsymbol{X_j}|\boldsymbol{\mathcal{S}_j})$ is the likelihood function

$$P(\boldsymbol{X_j}|\boldsymbol{\mathcal{S}_j}) = (2\pi\sigma^2_{\epsilon_j})^{-\frac{K}{2}} \exp\left(-\frac{||\mathcal{G}_j(\boldsymbol{\mathcal{S}_j}) - \boldsymbol{X_j}||^2}{2\sigma^2_{\epsilon_j}}\right). \tag{3.9}$$

Note that, if the noise ϵ_j is Gaussian-distributed with zero mean and constant variance $\sigma^2_{\epsilon_j} = (1/4)\ln^2 \mathrm{UF}_j$, the distribution (3.9) is a multivariate Gaussian function with mean vector $\mathcal{G}_j(\boldsymbol{\mathcal{S}_j})$ and scalar standard deviation σ_{ϵ_j}. A Markov-Chain Monte-Carlo method (MCMC) can be used to sample (3.8) and to yield the probability description of the vector-parameter space $\boldsymbol{\mathcal{S}_j}$, as detailed somewhere else (Kseib *et al.* 2011). Examples of input uncertainties obtained by using this method can be found in Najm *et al.* (2009) and Kseib *et al.* (2011).

It is worth emphasizing that in method $\mathcal{M}_2$ the uncertainty in $k_{f,j}$ is split into the three Arrhenius parameters. This implies the following subtle difference with respect to method $\mathcal{M}_1$. While a single realization using $\mathcal{M}_1$ gives a rate constant whose logarithmic value may become increased or decreased uniformly along the entire range of temperatures, a single realization in method $\mathcal{M}_2$ provides a rate constant whose value may vary with temperature in a substantially different manner from the way that the nominal rate constant does, especially if the activation energy contains a large degree of uncertainty. However, this method is limited by $\mathcal{L}_2$-$\mathcal{L}_4$, in that it does not account for cross-correlations between measurement uncertainties, it assumes temperature-independent uncertainties, and it cannot represent the influences of residual impurities in shock-tube measurements.

Method $\boldsymbol{\mathcal{M}_3}$) Methods $\mathcal{M}_1$ and $\mathcal{M}_2$ rely on the assumption that the noise ϵ_j along the $\ln k_{f,j}$ axis in the $\{1/T, \ln k_{f,j}\}$ plane is known. The final response of the combustion system depends on the choice of this noise representation. However, the justification for this assumption cannot be found in any physical grounds. A different approach is to superpose a given representation of the noise along the $Y_{p,j}$ axis in the experimental concentration time-history $\{t, Y_{p,j}\}_{T=T_o}$ of the monitored reactant in Figure 1(a). A noise model can be superposed on the concentration, in such a way that -for instance- $\sigma_{\epsilon_j} \sim (\overline{Y'^2_{p,j}})^{1/2}$. The assumption of a Gaussian noise model in the $\{t, Y_{p,j}\}$ plane may be justified on the grounds that the concentration time-history is retrieved directly from laser measurements, but it may not be justifiable after operations have been made to the experimental data as those required to translate them into a $\{1/T, \ln k_{f,j}\}$ plane of the type depicted in Figure 1(d). If, additionally, the noise ϵ_j is assumed to be stationary, its variance may be calculated -for instance- from the mean of the square of the concentration fluctuations, $\sigma^2_{\epsilon_j}(T_o) \sim \overline{Y'^2_{p,j}}|_{T=T_o}$. Therefore, although a model distribution for ϵ_j needs to be specified, in this method the variance of the noise is naturally characterized directly from the data and is allowed to vary with temperature. Additionally, no previous knowledge of the uncertainty factor UF_j is needed. Furthermore, the effects of the residual impurities in the shock tube are automatically accounted for.

Since the conservation equations (2.4) are non-linear, the operator $\boldsymbol{\mathcal{F}}$ in (3.1) becomes non-linear as well. In order to infer the probability density functions of the Arrhenius parameters from the uncertain concentration time history at each temperature, $\{t, Y_{p,j}\}_{T=T_o}$, a Bayesian inference strategy can be used. Consider the input-parameter vector $\boldsymbol{\mathcal{S}_j} = [\ln B_j, n_j, E_{a,j}, Y^0_{R,j}]^{\mathrm{T}}$, where $Y^0_{R,j}$ is the initial concentration of the equivalent species that simulates the effects of the impurities, and the experimental data vector $\boldsymbol{X} = [Y_{p,j}(t_1), \ldots Y_{p,j}(t_K)]^{\mathrm{T}}$ that is composed of the K measured data points at $T = T_o$ (and possibly also $P = P_o$ for termination reactions). If $F(\boldsymbol{\mathcal{S}_j}, t)$ represents the solution to (2.4) for a given set of kinetic parameters $\boldsymbol{\mathcal{S}_j}$ for step j, then the Bayesian-inference technique can be used to find the parameter vector $\boldsymbol{\mathcal{S}_j}$ that brings the model into agreement with the measurements up to the imposed noise ϵ_j, or equivalently, $F(\boldsymbol{\mathcal{S}_j}, t) = \boldsymbol{X_j} + \epsilon_j$. The inference of the input parameters can be performed by using Bayes' rule (3.8) and

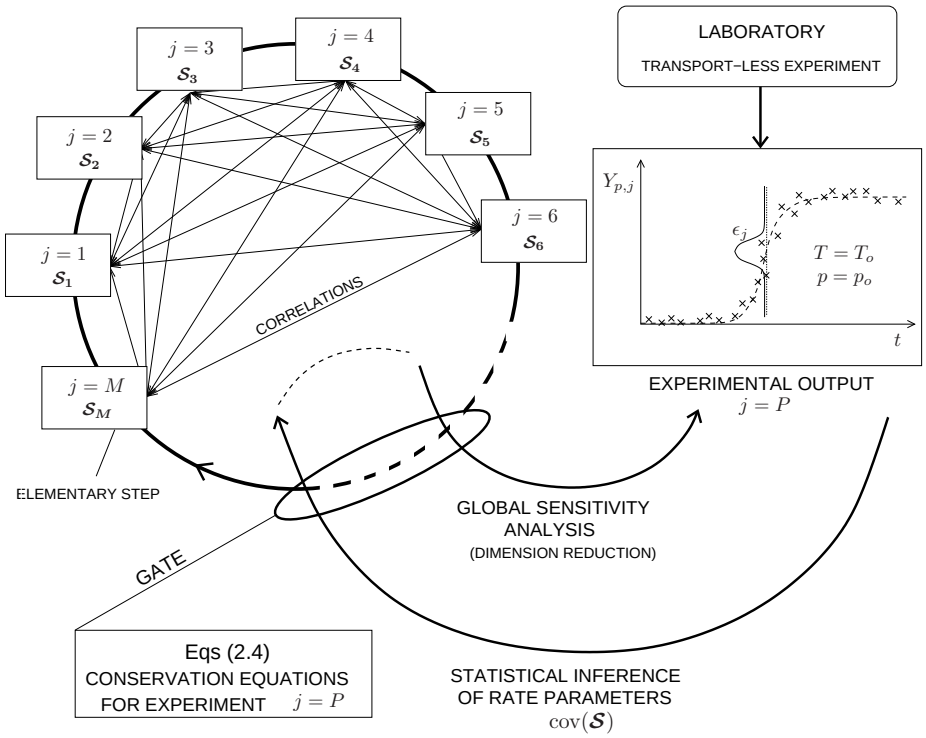

FIGURE 3. Schematics of method $\mathcal{M}_4$ -the active chemical mechanism- for quantifying uncertainties in reaction rates.

by sampling the likelihood function (3.9). From the MCMC method, the mean vector $\boldsymbol{\mathcal{S}_j}$ and the covariance matrix $\mathrm{cov}(\boldsymbol{\mathcal{S}_j})$ at each test temperature T_o can be calculated.

This method is limited solely by $\mathcal{L}_4$, in that it does not account for cross-correlations between measurement uncertainties. Earlier work (Miki *et al.* 2012) used a similar approach, without accounting for residual impurities, to characterize the uncertainties in step 1 of Table 1 by using experimental $\{t, Y_{p,j}\}$ data from Hong (2010).

Method $\mathcal{M}_4$) All three methods $\mathcal{M}_1 - \mathcal{M}_3$ described above belong to a generalized inference approach that is not limited by any of the $\mathcal{L}_1 - \mathcal{L}_4$ restraints outlined in Section 2.4. Figure 3 shows a schematics of such an approach, which is referred to as the *active chemical mechanism*. Subject to the existence and availability of sufficient experimental data, the active chemical mechanism updates the nominal values and uncertainties in the kinetic parameters through a cyclic procedure.

Experimental data from transport-less experiments can be injected through the cycle to infer the kinetic parameters. Numerical calculations of (2.4) are performed in conjunction with the active mechanism to reproduce the experimental concentration time-history of the monitored reactant $Y_{p,j}(t)$. By using equations (2.4) to represent the complex gas dynamics in the shock tube, the concept of "gate" in uncertainty quantification (Iaccarino *et al.* 2012) is being implicitly used, in that a model reduction is being undertaken based on physical grounds and all uncertainties in the experiments are being transferred into effective uncertainties in the source terms (2.1)-(2.2).

Using equations (2.4) and the active mechanism, a global sensitivity analysis assists in dimension reduction by identifying the critical kinetic parameters that influence the con-

Method	Limited by $\mathcal{L}_1$	$\mathcal{L}_2$	$\mathcal{L}_3$	$\mathcal{L}_4$	Describes the input uncertainty in terms of
$\mathcal{M}_1$	yes	yes	yes	yes	$P(A_j)$, $j = 1, \dots M$.
$\mathcal{M}_2$	no	yes	yes	yes	$P(A_j)$, $P(n_j)$, $P(E_{a,j})$, $P(A_j, n_j)$, $P(A_j, E_{a,j})$, $P(n_j, E_{a,j})$, for $j = 1, \dots M$.
$\mathcal{M}_3$	no	no	no	yes	$P(A_j)$, $P(n_j)$, $P(E_{a,j})$, $P(A_j, n_j)$, $P(A_j, E_{a,j})$, $P(n_j, E_{a,j})$, at $T = T_o$ and $p = p_o$, and for $j = 1, \dots M$.
$\mathcal{M}_4$	no	no	no	no	$P(A_j)$, $P(n_j)$, $P(E_{a,j})$, $P(A_i, n_j)$, $P(A_i, E_{a,j})$, $P(n_i, E_{a,j})$, at $T = T_o$ and $p = p_o$, and for $i = 1, \dots M$, $j = 1, \dots M$.

TABLE 2. Summary of methods proposed in this study for modeling input uncertainties in chemical rates. The symbol P denotes the probability density function.

centration time history $\{t, Y_{p,j}\}$. The global sensitivity to the parameter $\mathcal{S}_i$, with $\mathcal{S}_i$ the i-th component of the vector of kinetic parameters, is given by $R_i = \mathrm{var}[\mathrm{E}(Y_{p,j}|\mathcal{S}_i)]/\sigma^2_{\epsilon_j}$, where E denotes the expectation operator. Note that R_i is, in general, a function of time t and of the thermodynamic conditions T_o and p_o. Additionally, R_i provides the weighted measure of the sensitivity of $Y_{p,j}(t)$ to the parameter S_i, in that its definition accounts for the amount of variability in $\mathcal{S}_i$. For this reason, the calculation of R_i requires the knowledge of the probabilistic distributions of the kinetic parameters. If these distributions are unknown, as for instance when the cycle starts, local sensitivities of the type $r_i = (\overline{\mathcal{S}_i}/Y_{p,j})(\partial Y_{p,j}/\partial \mathcal{S}_i)$ can be used in a first approximation as traditionally done in the design and assessment of kinetic-isolation experiments (Davidson *et al.* 1996; Hong 2010). Once the set $\boldsymbol{\mathcal{S}_r}$ of most sensitive kinetic parameters has been isolated, Bayesian inference methods can be used to infer their updated values and uncertainties as described in method $\mathcal{M}_3$, by simply substituting $\boldsymbol{\mathcal{S}_j}$ in that formulation by $\boldsymbol{\mathcal{S}_r}$, thereby automatically yielding the cross-correlation structure among all the retained kinetic parameters. In this method, the operators $\boldsymbol{\mathcal{F}}$ and $\boldsymbol{\mathcal{G}}$ in (3.1)-(3.2) can be fully nonlinear. This strategy is not affected by any of the limitations $\mathcal{L}_1 - \mathcal{L}_4$.

4. Conclusions

In this study, four main limitations of state-of-the-art approaches for quantifying uncertainties in rate constants were outlined, which concerned $\mathcal{L}_1$) the lack of modeling of uncertainties in all three Arrhenius parameters, $\mathcal{L}_2$) the temperature-independence of the uncertainty, $\mathcal{L}_3$) the lack of modeling of the effects of residual impurities on the measurements, and $\mathcal{L}_4$) the resulting uncorrelation among the uncertainties in elementary rate constants. To suppress these limitations, four methods $\mathcal{M}_1 - \mathcal{M}_4$ of increasing complexity were proposed to quantify uncertainties in reaction rates, the outputs of which are summarized in Table 2. These methods provide physics-based formulations for modeling uncertainties in reaction rates, and further research is being undertaken to compare their performances.

As detailed in Urzay *et al.* (2012), non-intrusive methods of chemical-kinetic uncertainty quantification in high-speed turbulent combustion utilize as inputs single realiza-

tions of the stochastic space of rate constants $\boldsymbol{\mathcal{K}}$. It should not be denied that, in addition to high-fidelity calculations, serious endeavors in uncertainty quantification also require high-fidelity inputs if physically-meaningful analyses of the effects of the uncertainties are pursued. In particular, suitable methods for quantifying input uncertainties in chemical kinetics need to satisfy realizability constraints in the rate constants $k_{f,j}$ which must be in accord with the corresponding physics. It is known from the kinetic theory of gases that the rate constants vary smoothly with temperature and pressure (Vincenti & Kruger Jr. 1965). In all methods $\mathcal{M}_1 - \mathcal{M}_4$ outlined above, implicit realizability conditions on the derivatives $\partial k_{f,j}/\partial T|_p$ and $\partial k_{f,j}/\partial p|_T$ are automatically enforced by equations (2.4) and (3.3)-(3.5), which are mathematical representations of the rate-determining experiments and of some of the underlying gas-kinetic phenomena. Whether or not these constraints are sufficient is a topic of current research. However, methods $\mathcal{M}_1 - \mathcal{M}_3$ do not satisfy any physical realizability constraints related to cross-correlations among the uncertainties in rate constants. Further research is needed to quantify these cross-correlations and to assess their relevance in combustion calculations under chemical-kinetic uncertainties.

Acknowledgments

This investigation was funded by the Predictive-Science Academic-Alliance Program (PSAAP), Grant # DE-FC52-08NA28614, for investigating uncertainties in hydrogen-fueled SCRAMJETS. The authors are indebted to Dr. Schiavazzi for useful comments in earlier drafts. The first author was supported by the 2011-2012 Postdoctoral Fellowship for Excellence in Research, Ibercaja Foundation (Zaragoza, Spain).

REFERENCES

Baulch, D. L., Bowman, C. T., Cobos, C. J., Cox, R. A., Just, T., Kerr, J. A., Pilling, M. J., Stocker, D., Troe, J., W., T., Walker, R. M. & Warnatz, J. 2005 Evaluated kinetic data for combustion modeling: Suplement ii. *J. Chem. Phys. Ref. Data* **34** (3), 757–1397.

Davidson, D. F. & Hanson, R. K. 2004 Interpreting shock-tube data. *Int. J. Chem. Kin.* **36** (9), 510–523.

Davidson, D. F., Petersen, E. L., Röhrig, M., Hanson, R. K. & Bowman, C. T. 1996 Measurement of the rate coefficient of $H + O_2 + M \rightarrow HO_2 + M$ for M = Ar and N_2 at high pressures. *Proc. Comb. Inst.* **26**, 481–488.

Davis, S., Joshi, A., Wang, H. & Egolfopoulos, F. 2005 An optimized kinetic model of H_2/CO combustion. *Combustion and Flame* **30**, 1283–1292.

Hong, Z. 2010 *An improved hydrogen/oxygen mechanism based on shock tube/ laser absorption measurements.* Ph.D. Thesis, Stanford University.

Hong, Z., Davidson, D. F. & Hanson, R. K. 2011 An improved H_2/O_2 mechanism based on recent shock tube/laser absorption measurements. *Comb. Flame* **158**, 633–644.

Iaccarino, G., Sharp, D. & Glimm, J. 2012 Quantification of margins and uncertainties using multiple gates and conditional probabilities (To appear in *Reliab. Eng. Syst. Safety*) .

Konnov, A. A. 2008 Remaining uncertainties in the kinetic mechanism of hydrogen combustion. *Comb. Flame* **152**, 507–528.

Kseib, N., Urzay, J. & Iaccarino, G. 2011 Statistical inference of uncertainties in

elementary reaction rates of chemical mechanisms. *Annual Research Briefs*, Center for Turbulence Research, NASA Ames/Stanford University pp. 1–8.

Miki, K., Cheung, S. H., Prudencio, E. & Varghese, P. 2012 Bayesian uncertainty quantification of recent shock tube determinations of the rate coefficient of reaction $H + O_2 \leftrightharpoons OH + O$. *Int. J. Chem. Kin.* **44**, 586–597.

Mueller, M. E., Iaccarino, G. & Pitsch, H. 2012 Chemical kinetic uncertainty quantication for large eddy simulation of turbulent nonpremixed combustion. *Proc. Comb. Inst.* **34**, 1–8.

Najm, H. N., Debusschere, B. J., Marzouk, Y. M., Widmer, S. & Le Maitre, O. P. 2009 Uncertainty quantification in chemical systems. *Int. J. for Numer. Meth. Eng.* **80**, 789–814.

Reagan, M. T., Najm, H. N., Ghanem, R. G. & Knio, O. M. 2003 Uncertainty quantification in reacting-flow simulations through non-intrusive spectral projection. *Comb. Flame* **133**, 545–555.

Sheen, D. A. & Wang, H. 2011 Combustion kinetic modeling using multispecies time histories in shock-tube oxidation of heptane. *Comb. Flame* **158**, 645–656.

Urzay, J., Kseib, N., Palacios, F., Larsson, J. & Iaccarino, G. 2012 A stochastic flamelet progress-variable approach for numerical simulations of high-speed turbulent combustion under chemical-kinetic uncertainties. *Annual Research Briefs*, Center for Turbulence Research, NASA Ames/Stanford University .

Vincenti, W. G. & Kruger Jr., C. H. 1965 *Physical Gas Dynamics.* John Wiley & Sons.